Computers and Structures 86 (2008) 2079–2086

Contents lists available at ScienceDirect

Computers and Structures

journal homepage: www.elsevier.com/locate/compstruc

Penetration prediction of missiles with different nose shapes by the discrete element numerical approach

Wenjie Shiu *, Frédéric Victor Donzé, Laurent Daudeville

Joseph Fourier University, Soils Solids Structures Laboratory, BP53, 38041 Grenoble cedex 9, France

ARTICLE INFO

Article history:
Received 26 February 2007
Accepted 12 March 2008
Available online 3 July 2008

Keywords:
Discrete element method
Penetration depth
Concrete slab
Nose shape of missile

ABSTRACT

A three dimensional numerical model based on the discrete element method (DEM) is developed to predict the penetration depth caused by a non-deformable missile against a reinforced concrete slab. Initial calibration of the model was done with a series of flat-nose missile tests. Additional simulations were performed with varying shapes for the missile's nose. The present numerical model is compared to experimental test data provided by the French Atomic Energy Agency (CEA) and the French Electrical power Company (EDF). For thin concrete slabs, the evolution of the penetration depth in terms of the nose shape predicted by the DEM agrees more with the experimental data than the evolution predicted by Chen and Li's empirical law.

1. Introduction

Reinforced concrete structures are often used as protection against hazardous impacts, such as aircraft crashes, mountainous rock falls, accidental explosions and other events. A highly reliable prediction model is the key point to deal with this kind of problem. These models consider four major quantities [7,10] which measure the local impact effects on a concrete structure: the penetration depth, the scabbing, the perforation and the ballistic limits. The penetration depth is the distance a projectile penetrates a thick concrete target without resulting in perforation and scabbing. The perforation or scabbing limit is the minimum thickness of the target to prevent perforation or scabbing and the ballistic limit is the minimum initial impact velocity to perforate the target.

The empirical formulae are widely used to assess the penetration, scabbing and perforation. Previous reviews of these empirical formulae have been investigated [1,15,22]. Some of these, such as the Modified NDRC formula [13] and perforation limit [3] have been accepted as useful to study local impact problems such as penetration depths.

However, since most of the available empirical formulae were obtained by data-fitting of experimental tests, the use of the formulae was limited by the range of parameters tested such as the missile's mass and the impact velocity. Moreover, as some of them are dimensionally non-homogenous and unit dependent, they provide little physical meaning about the local impact event [14]. The experimental tests are often carried out with a series of missiles for which the nose shape is poorly defined. Hence, the effect of this parameter on the penetration depth is difficult to determine. A numerical approach is developed in this work to overcome the shortcomings of these empirical formulae, and to provide a better understanding of the problem.

The discrete element method (DEM) [6], which is an alternative numerical method to continuum-type methods [2], is used here to study the behavior of concrete structures subjected to rigid impacts. This method does not rely upon any assumption about where and how a crack or several cracks occur and propagate, since the medium is naturally discontinuous and is very well adapted to dynamic problems, when a transition from the solid state to a granular flow regime is observed.

Nevertheless, when a DEM model is used, the issue of the modeling scale has to be addressed: the DEM is well adapted to the modeling of granular material, where an element represents a grain [6,12]. Numerous authors have also used the DEM to simulate cohesive geomaterials such as concrete, at the heterogeneity scale [19,20], i.e. the size of an element is on the order of the size of the biggest heterogeneity. This approach gives a better understanding of concrete fracture, but makes the modeling of real structures difficult because of the computational cost. Another way to use the DEM consists in using a higher scale model, which considers that the whole collection of elements must reproduce the macroscopic behavior of concrete. Such an approach was mainly developed in 2D [16,18] or in 3D with a regular assembly of discrete elements [21].

The bases of the 3D DEM model and the local parameter identification process [9] are given in Section 2. This model is then applied to simulate the impact of a rigid missile on a reinforced concrete slab. This configuration is based on the experimental CEA-EDF tests [3]. In the first series of experimental tests, the nose

* Corresponding author. Tel.: +33 4 56528642; fax: +33 4 76827043.
E-mail address: wen-jie.shiu@hmg.inpg.fr (W. Shiu).

0045-7949/$ - see front matter
doi:10.1016/j.compstruc.2008.03.003

Nomenclature

$A_{(i)}$	the generalized acceleration
D	the diameter of the missile
E_c	Young's modulus for concrete
E_s	Young's modulus of the steel reinforcement
F_i	the ith component of the generalized contact force
$F^d_{(i)}$	the damping force
f_c	the compressive stress of a concrete target
g	the gravitational acceleration
I	the moment of inertia
I_d	the impact function $\left(=\frac{Mv^2}{D^3 f_c}/82.6 f_c^{-0.544}\right)$
J	the polar moment of the disk's cross-section (between two bonding elements)
K_i	the ith component of the element stiffness
K_n	the normal stiffness of the element
$\bar{k}^n$	(also noted Pb_kn) the normal stiffness of the parallel bond
K_s	the tangent stiffness of the element
$\bar{k}^s$	(also noted Pb_ks) the tangent stiffness of the parallel bond
k	the dimensionless penetration depth
M	the mass of the missile
M_i	the generalized moment acting on each element
$\overline{M}_i^n$	the normal generalized moment acting on each parallel bond
$\overline{M}_i^s$	the tangent generalized moment acting on each parallel bond
m	the mass of the element
N_d	the geometry function $\left(=\frac{M}{\rho_c D^3}\right)$
Pb_nstrength	parallel bond maximum normal stress
Pb_sstrength	parallel bond maximum shear stress
U_i	the overlap between two elements in contact
v	the impact velocity
X	the penetration depth
$\ddot{x}_i$	the translation acceleration

Greek symbols

α	numerical damping factor
μ	the friction coefficient
$\Delta\theta^n$	the normal relative angular rotation between two elements in contact
$\Delta\theta^s$	the tangent relative angular rotation between two elements in contact
$\dot{\omega}_i$	the rotational acceleration
ρ_c	the density of a concrete target

of the missile is flat. The numerical and experimental results were compared in terms of the missile's trajectory. Then, using the same local parameters in the numerical model, additional simulations were performed to study the effects of varying nose shapes.

2. The DEM model

Following impact simulations in which the SDEC code was used [16,4], the potential of the PFC^{3D} code [11] to simulate real test cases is now investigated.

In the PFC^{3D} code, the discrete elements are spherical and interact with a force–displacement type law, (see Eq. (1a)). The equations of motion applied to each element are defined by Eqs. (1b) and (1c).

$$F_i = K_i U_i, \tag{1a}$$

$$F_i = m(\ddot{x}_i - g_i) \text{ (translational motion)}, \tag{1b}$$

$$M_i = I\dot{\omega}_i \text{ (rotational motion)}, \tag{1c}$$

where F_i is the ith component of the contact force, K_i the stiffness associated to each element, with K_n in the normal direction and K_s in the tangent direction, U_i is the overlap between two elements in contact, m is the mass of each element, $\ddot{x}$ and $\dot{\omega}$ are the translational acceleration and rotational acceleration respectively, g is the gravitational acceleration, M_i is the resultant moment acting on each element and I is the moment of inertia. During the calculation cycle, the force–displacement law (Eq. (1a)) is calculated first, then the new element's position will be updated by the law of motion (Eqs. (1b) and (1c)). Note that more information about the formulation of PFC^{3D} can be found in [11].

PFC^{3D} provides two ways of formulating the interaction between two elements: the contact and parallel bonds. Because the present objective was to simulate concrete which is a frictional–cohesive material, the parallel bond has been chosen for the numerical modeling since it can transfer both the contact force and moment between two elements in contact. The parallel bond is to be treated as glue lying on a finite circular cross-section between two elements. To form a parallel bond, its stiffness and yield stress should be defined before the calculation as well. Thus new intrinsic parameters are involved, such as, pb_kn, pb_ks, pb_nstrength, pb_sstrength which are normal and tangent stiffness, and normal and shear yield stress respectively. The stress which acts on the parallel bond was calculated via the beam theory (see Fig. 1). If either of the maximum stresses exceeds its corresponding bond resistance, the parallel bond breaks. Thus a simple elastic–brittle behavior was used here. The transferring force in a parallel bond is described in Eq. (2) by replacing the stiffness terms by pb_kn and pb_ks. The moment transfers between two bonded elements is calculated by

$$\overline{M}_i^n = \bar{k}^s J \Delta\theta^n, \tag{2.a}$$

$$\overline{M}_i^s = \bar{k}^n I \Delta\theta^s, \tag{2.b}$$

where $\overline{M}_i^n$ and $\overline{M}_i^s$ are the normal and tangent generalized moments, $\bar{k}^n$ and $\bar{k}^s$ are the normal and the tangent stiffnesses of the parallel

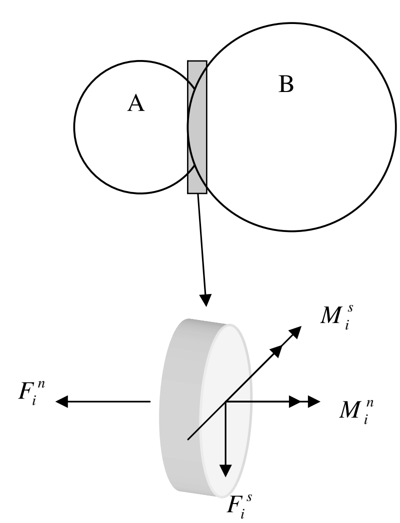

Fig. 1. Force and moment components of a parallel bond cohesive interaction.

bond, J is the polar moment of the disk's cross-section, I is the moment of inertia of the disk's cross-section, $\Delta\theta^n$ and $\Delta\theta^s$ are the normal and the tangent relative angular rotation between two elements in contact. Furthermore, when a parallel bond exists between two elements, slip may occur between these bonded elements.

Energy dissipation was also used in our numerical model. The energy involved between two interacting elements is dissipated through frictional sliding for which a Coulomb friction coefficient μ is defined. Moreover, a local non-viscous damping is available in PFC^{3D}, where the damping force is put together with the equation of motion such that

$$F_{(i)} + F^{d}_{(i)} = M_{(i)}A_{(i)}; \tag{3}$$

where $F(i)$, $M(i)$, and $A(i)$ are the generalized force, mass and acceleration components respectively, and $F^{d}_{(i)}$ is the damping force

$$F^{d}_{(i)} = -\alpha|F_{(i)}|\mathrm{sign}(V_{(i)});$$
$$\mathrm{sign}(y) = \begin{cases} +1, & \text{if } y > 0; \\ -1, & \text{if } y < 0; \\ 0, & \text{if } y = 0; \end{cases} \tag{4}$$

where α is the numerical damping (the detailed description can be found in the PFC^{3D} manual). After some pre-process numerical simulation tests, the numerical damping factor is set to 0.15 and 0.05 for the concrete element and the reinforcement element respectively.

2.1. Local parameters identification process

The goal is to model a structure, in which some of the macroscopic material properties (Young's modulus, Poisson's ratio, tensile and compressive strengths) are known. The structure's geometry is discretized with a collection of discrete elements. To each of these elements a set of local parameters is assigned so that the macroscopic behavior of this collection is representative of the real material. For example, the values of the normal and shear stiffnesses are chosen locally to get the corresponding macro stiffnesses, namely Young's modulus and Poisson's ratio. This procedure is fully described in [9] and is based on the simulation of quasi-static uniaxial compression/traction tests. A tri-axial test model is pre-developed in PFC^{3D} and for a standard-sized specimen:

- A compact, polydisperse discrete element collection is generated.
- An elastic compression test is run with local elastic parameters given by the "macro–micro" relations.
- Compressive and tensile rupture axial tests are simulated to deduce the remaining local parameters.

By performing these tests, the local parameters kn, ks, pb_kn, pb_ks, pb_nstrength, pb_sstrength are set such that the global mechanical properties of the collection of discrete elements are, as close as possible, to those of concrete with a 35 GPa Young's modulus and a 30 MPa compressive strength. The wave propagation velocity can be checked when the impact occurs. As for the strain rate effect, it has been shown that in the compressive mode, the inertial response of the medium plays a major role [8]. However, when simulating the first impact test, some readjustments, mainly the damping value, were needed to fit the experimental data set. This readjustment procedure was performed only once and the exact same set of parameters was used in all subsequent impact test cases to demonstrate the predicting capability of the method. The input numerical data are given in Tables 1 and 2.

2.2. Introducing reinforcement

As in work by other authors [17,18], reinforcement bars are represented as lines of elements placed next to one another, which have the same diameter as the diameter of the rebar. In the CEA-EDF test data, there are four reinforcement layers placed at equal-distances in the concrete target slab. The same geometrical configuration is used in the numerical model and parallel bonds are used between the rebar elements.

In terms of the local behavior of the reinforcement elements, a simplified model is used here: instead of the elastic–plastic behavior observed in steel rebars only an elastic–brittle behavior is considered, because plasticity is not defined in PFC^{3D}. To overcome this limitation while keeping the same amount of cohesion energy, the rupture threshold of the elastic–brittle behavior law has been artificially increased. Thus, to limit the amount of kinetic energy released during the local brittle fracturing process, a non-viscous damping component is added.

2.3. Discrete element modeling

The concrete target slab: The reinforcement pattern is shown in Fig. 2. The isotropic and polydisperse packing of "concrete" elements is obtained through a disorder technique available in PFC^{3D}, around the reinforcement lines. A parallel bond was applied between the concrete elements.

The following procedure was used to set up the model:

1. Generate six walls (a box) which correspond to the edges of the target, i.e. 1.46 m × 1.46 m × 0.208 m, (as to tests D35 and D37, the box size should be replaced by 1.46 m × 1.46 m × 0.416 m).
2. Generate the reinforcement elements and set their transition and rotation ability to zero.
3. Generate the concrete elements keeping the same size distribution as in the quasi-static test. During this step, all movement between concrete elements is allowed, and the algorithm stops when equilibrium is reached.
4. Set the parallel bonds between all concrete elements, and then delete the front wall and the back wall which correspond to the impact direction.
5. Release the reinforcement elements.

This procedure is followed to avoid obtaining an undesirable residual contact force between two elements during the DE gener-

Table 1
Parameters used in the model for concrete (nomenclature of PFC^{3D} is used)

Parallel-bond normal stiffness Pb_kn (Pa/m)	70×10^9
Parallel-bond shear stiffness Pb_ks (Pa/m)	14×10^9
Parallel-bond maximum normal stress Pb_nstrength (Mpa)	230
Parallel-bond maximum shear stress Pb_sstrength (Mpa)	23
Numerical damping α	0.05
Friction coefficient μ	0.3
Density ρ_c (kg/m^3)	2500

Table 2
Parameters used in the model for the steel reinforcement (nomenclature of PFC^{3D} is used)

Parallel-bond normal stiffness Pb_kn (Pa/m)	$21{,}000 \times 10^9$
Parallel-bond shear stiffness Pb_ks (Pa/m)	5250×10^9
Parallel-bond maximum normal stress Pb_nstrength (Mpa)	3500
Parallel-bond maximum shear stress Pb_sstrength (Mpa)	1250
Numerical damping α	0.15
Friction coefficient μ	0.3
Density ρ_c (kg/m3)	28,000

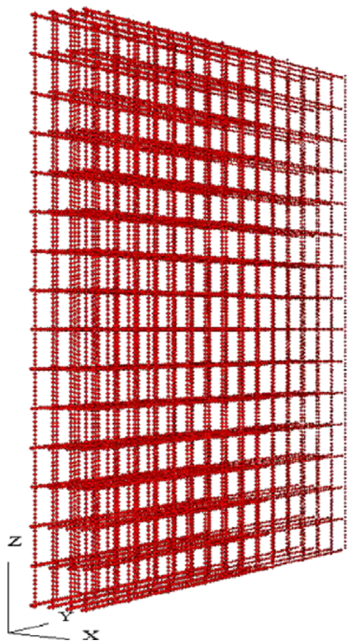

Fig. 2. The four reinforcement layers of the concrete slab, represented by a set of 17,408 discrete elements.

ation. The total number of discrete elements in the concrete slab is 19,403, with a radius distribution size between 0.005 m and 0.02 m. This resolution size was chosen based on the rebar's diameter, which imposed the minimum discrete element size. Once this size has been fixed, the identification of the local mechanical properties were set up and kept constant for the impact simulation.

Studies of size effect were not carried on here.

The block: Its geometry is as close as possible to the experimental one. The "clump" command has been used to simulate the missile, thus all the elements located in this clump can move together as well, so the missile was treated as a rigid body. The diameter and the weight of the missile are kept the same as in the CEA-EDF test, and the local stiffnesses is chosen to be identical to those of the rebars, since it is made of steel.

Computation conditions: Prior to and during any computation, gravity is applied on the slab until equilibrium is reached. The block is initially placed just above the slab surface, with the initial velocity corresponding to its impact velocity. The impact configuration (position and orientation) has been set as close as possible to the observed experimental configuration. On each side, a layer of 10 cm is fixed during the calculation. This gives a boundary condition. The block is subjected to gravity as well (Fig. 3).

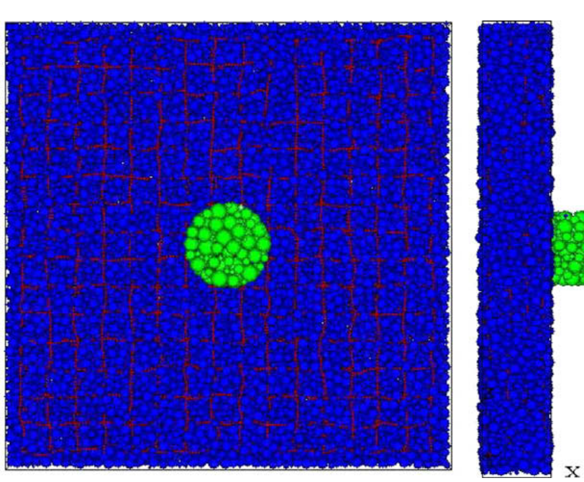

Fig. 3. On the left, a front view of the initial configuration of the impact process, on the right, a side view. Because of the coarse size of the concrete discrete elements, the first reinforcement layer is visible. Both the concrete slab and the impactor are subjected to gravity.

3. Modeling of impact tests

3.1. CEA-EDF tests

The experimental shots were performed by the French Atomic Energy Agency (CEA) and the French Electrical power Company (EDF) on reinforced concrete slabs, the thickness of which was chosen to represent, in a realistic way, the thickness of the wall of a reactor containment [3]. Seven tests have been chosen among all the CEA-EDF tests for the numerical simulation. The properties of the concrete material and the geometric shape of the missile (flat nose) were kept constant. The effects of parameters such as the missile velocity (25–450 m/s), its mass (20–300 kg), the ratio of the missile diameter to the thickness of the slab (0.24–2.9) and characteristics of the steel reinforcement were studied (Tables 3 and 4).

3.2. Numerical results

The results of the tests involving a 1.46 m × 1.46 m concrete slab with a 0.208 m thickness reinforced by four different steel layers, impacted by a 34 kg non-deformable flat nose missile with a diameter of 0.278 m at velocities of 102, 151 and 186 m/s were selected to be compared with the numerical model (tests D22, D24, D30). These velocities led to scabbing, penetration and perforation of the slab, respectively.

The block is initially placed just beside the slab surface, with the initial velocity corresponding to its impact velocity. The impact configuration (position and orientation) has been set as close as possible to the observed experimental configuration (Fig. 3).

The first results shown were obtained with the simulation of three tests with different impact velocities (102, 151 and 186 m/s, see Fig. 4). The other parameters are the same for all three tests. The model can describe the different observed configurations such as, perforation, scabbing and penetration.

As soon as the damping factor is set for one of these tests, the model is capable of predicting the trajectory of the missile for the other two cases. Thus, when fixing the damping parameter for the test D22 (151 m/s), which induces penetration and scabbing processes, the model was able to reproduce the slight penetration for the 102 m/s impact velocity and the perforation process for the 186 m/s impact velocity (Fig. 5).

The penetration depth was also calculated after numerical simulation for tests involving a simple penetration (no perforation had occurred; test D22, D28, D35), because these penetration test data are difficult to obtain, our numerical penetration results have been compared with the penetration prediction formula proposed in [5] which has been deemed reliable in recent years.

$$\frac{X}{D} = \sqrt{\frac{(1+k\pi/4N)}{(1+I_d/N_d)}\frac{4k}{\pi}I_d}, \quad \text{for } \frac{X}{D} \leqslant k, \tag{5.a}$$

$$\frac{X}{D} = \frac{2}{\pi}N_d \ln\left[\frac{1+I_d/N_d}{1+k\pi/4N_d}\right] + k \quad \text{for } \frac{X}{D} > k, \tag{5.b}$$

where X is the penetration depth, D is the diameter of the missile, k is the dimensionless penetration depth, as a flat nose missile is used here, k is equal to 0.707, and two dimensionless numbers: the impact function I_d and the geometry function N_d which are defined as $I_d = \frac{Mv^2}{D^3 f_c}/82.6 f_c^{-0.544}$, $N_d = \frac{M}{\rho_c D^3}$ for a flat nose missile, where M is

Table 3
CEA-EDF tests – concrete slabs

Shot	Concrete slab		Observation	
	Thickness (m)	Strength (Mpa)	Perforation (by PFC3D)	Penetration (m) (by Eq. (5))
D22	0.208	41.5	Yes	x
D24	0.208	38	No	0.05
D30	0.208	43.5	Yes	x
D27	0.208	44	Yes	x
D28	0.208	43.5	No	0.14
D35	0.416	38.5	No	0.285
D37	0.416	50	Yes	x

Table 4
CEA-EDF tests – missiles

Shot	Mass (kg)	Diameter (m)	Velocity (m/s)	Momentum (kg m s^{-1})	Kinetic energy (kgm^2 s^{-2})
D22	34	0.278	151	5.13E + 03	3.88E + 05
D24	34	0.278	102	3.47E + 03	1.77E + 05
D30	34.5	0.278	186	6.42E + 03	5.97E + 05
D27	51.6	0.3	129	6.66E + 03	4.29E + 05
D28	32.8	0.3	153	5.02E + 03	3.84E + 05
D35	31	0.3	445	1.38E + 04	3.07E + 06
D37	303	0.1	49	1.48E + 04	3.64E + 05

the mass of the missile, ρ_c is the density of a concrete target, v is the impact velocity and f_c the compressive stress of a concrete target.

Chen and Li [5] have also proposed a prediction formula for a small penetration depth, i.e., when $X/D < 0.5$ the following equation should be used:

$$\frac{X_{\text{test}}}{D} = 1.628\left(\frac{X_{\text{anal}}}{D}\right)^{2.789} \tag{5.c}$$

The numerical results show a good agreement with Eqs. (5a, b, c) (where Eq. (5.c) was used for test D24, see Table 3). This is true up to test D35 which involves a thicker target (0.416 m). This could be due to the lack of plasticity in the reinforcement as well as the fact that ductility is not imposed in the concrete used in the numerical model. All in all the difference between the numerical results and the prediction formula for test D35 is about 20%.

After having identified the local parameters as explained previously, calibrated the damping parameter with the 151 m/s impact velocity test, and shown that the model can predict the slab's response at different impact velocities, the influence of the nose shape is studied and compared to the penetration prediction formula proposed by Chen and Li [5].

3.3. Influence of the nose shape of missile

The nose shape of missile plays an important role when a missile strikes against a reinforced concrete wall. In particular, the impact force may vary. Most empirical prediction formulae are obtained by applying regression formulae to available experimental test data. To account for the shape of the nose, a coefficient is used. For example, in the modified NDRC formulae [13], the impact factor takes on the values of 0.72, 0.84, 1.0 and 1.14 for flat, blunt, spherical and sharp noses respectively. However, these geometrical characterizations are loosely constrained. To overcome this lack of constraint, an analytical nose shape function to interpret the contact force between the missile and the target during impact was suggested [5].

In the present paper, a comparison is done between Chen and Li's formulation [5] and the DEM in terms of the penetration ability. The investigation was limited to conical noses of varying

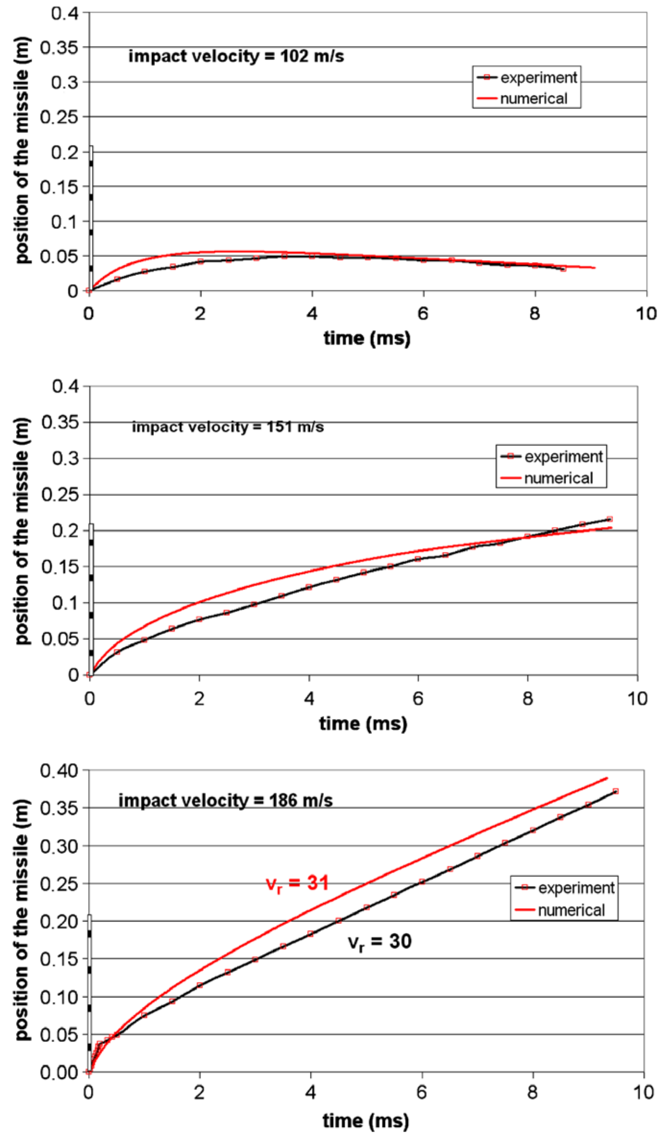

Fig. 4. Comparisons between simulations and experiments for the three impact velocities: 102, 151 and 186 m/s. V_r is the residual velocity of the missile after perforation.

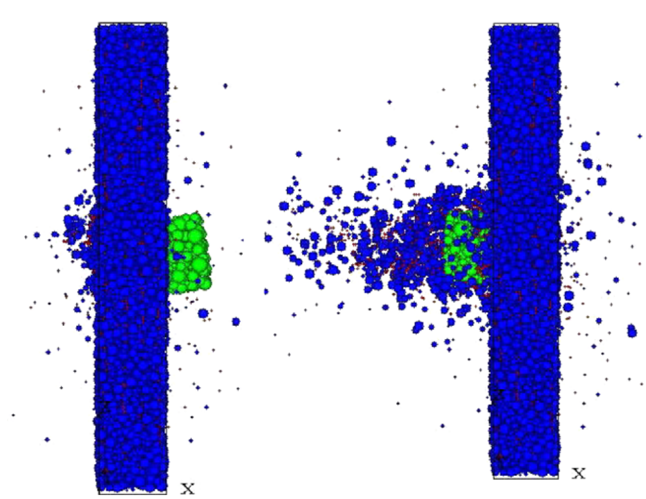

Fig. 5. On the left, a flat nose missile penetrates at 102 m/s impact velocity (snap at 8.405 ms). On the right, the impact velocity is 186 m/s impact velocity (snap at 9.3 ms). The same results are obtained experimentally.

Table 5
Results of experimental and numerical tests

	Target thickness (m)	Nose shape	Impact velocity (m/s)	Penetration depth (cm)
Experimental	0.4	Conic	88	23
	0.4	Conic	82	20
	0.4	Flat	90	17–20
Numerical	0.4	Flat	90	17
	0.4	Conic 0.1	90	14.3
	0.4	Conic 0.2	90	23
	0.4	Conic 0.25	90	27
	0.8	Flat	90	7.3
	0.8	Conic 0.1	90	14.2
	0.8	Conic 0.2	90	19.9
	0.8	Conic 0.25	90	25

lengths. A reference test case using a flat nose will be the starting point of the numerical data set.

Table 5 gives the experimental CEA-EDF test data used. Note that among all the existing tests, only one experimental impact shot which corresponds to the numerical configuration was launched with a conical nose shape, which will serve as comparison. A rigid-flat-nose has been chosen for the numerical simulation as a reference case, in which the mass is 227 kg, the impact velocity is 90 m/s and the diameter is 0.305 m. Then, the other three missiles have been generated with different nose lengths (0.1 m, 0.2 m 0.25 m) while keeping the same mass, the diameter and impact velocity. The target's thickness is 0.4 m, and it is simulated in the same way as before, i.e. keeping the same local parameters: kn, ks, pb_kn, pb_ks, etc. Four reinforcement layers were generated, and were placed in the concrete target in the same way as in the experimental set. The results are shown in Figs. 6 and 7. Chen and Li's [5] formula predicts that the sharper the nose shape, the greater the penetration depth. One might have thought that, as long as the impact kinetic energy consumed was the same, it

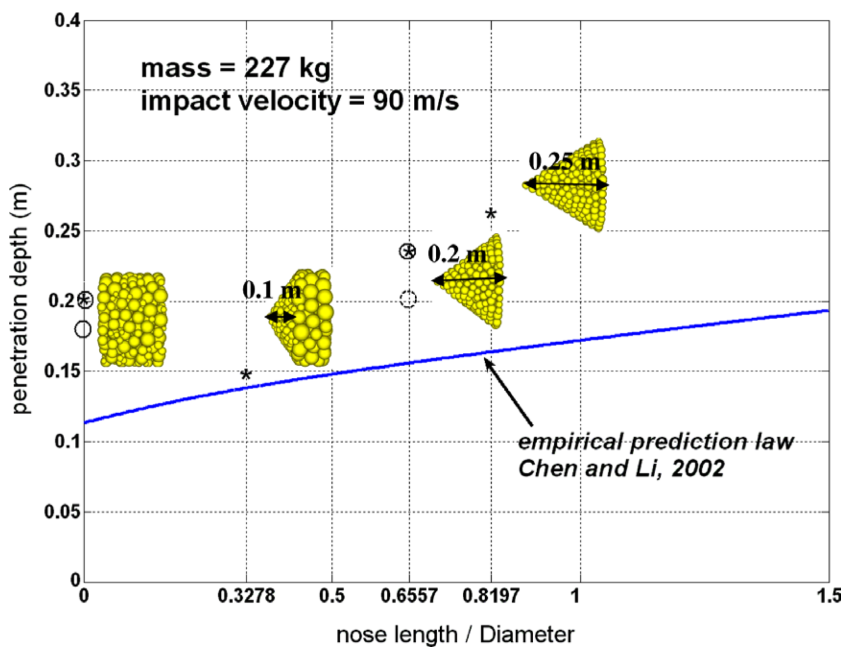

Fig. 6. Penetration depth vs missile's nose shape. The stars correspond to the numerical results. The circles correspond to the experimental tests presented in Table 5. The dashed circle corresponds to an impact velocity of 82 m/s.

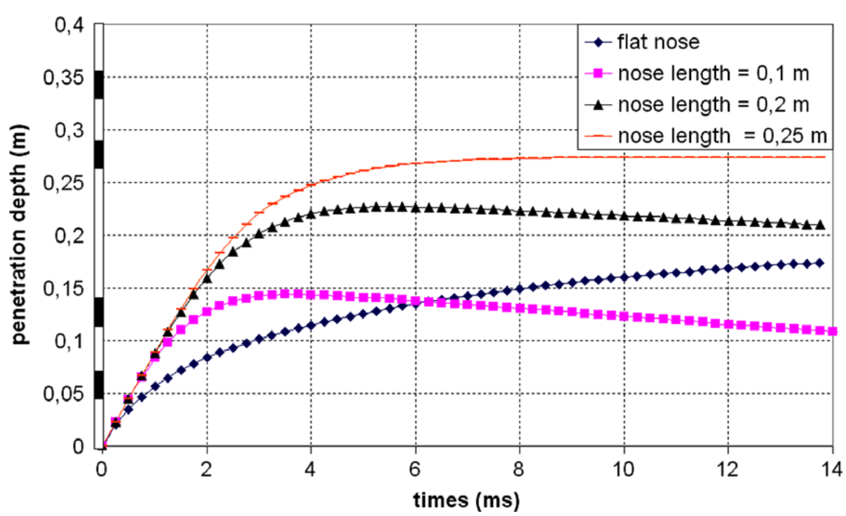

Fig. 7. Missile's trajectory history (numerical results).

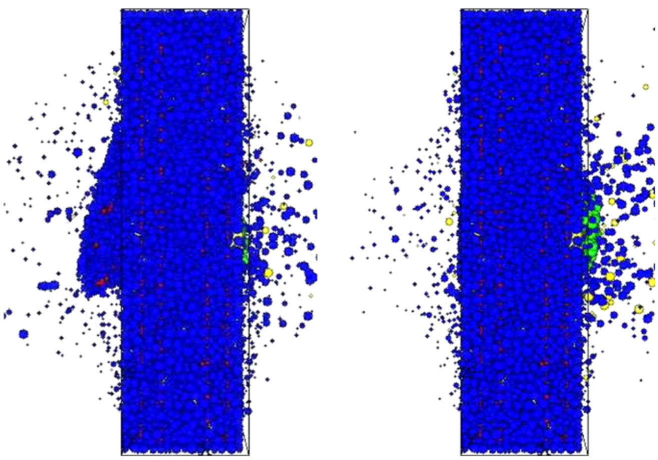

Fig. 8. Images captured at the end of the simulation for a flat-nose and a 10 cm nose length on the left side and right side respectively.

would be easier for a sharper nose to penetrate into a target. However, the numerical results in the present test conditions show that a flat-nose shape has a more significant penetration depth than that of a missile with a 10 cm nose length. This could be due to the effect of the plane wave propagation. When a missile strikes a concrete target, the impact energy converted into a pressure wave is greater for a flat-nose missile than for a conical nose missile. When the thickness of the target is of the same order as the missile's diameter, the amplitude of the transmitted wave may generate opposite face scabbing thus creating internal fracturing. The scabbing is due to the reflected waves. Because of this internal fracturing process, the missile's progression will be eased. This is exactly what is happening here, with a ratio between the target thickness and the missile diameter of 0.4 m–0.305 m. Fig. 8 shows the images captured after the impact where scabbing is observed in the opposite face of the slab for the flat-nose missile. On the same figure, the conical missile is less damaging.

Looking at snap shots of the displacement field, recorded at different time steps, for both the flat and conical nose missiles, as in Fig. 9, combined with the trajectory of the missile, see Fig. 7, one can see the effects of the damage on the progression of the missile. At $t = 3$ ms, the 0.1 m conical nose missile has already reached its maximum penetration depth. After that it rebounds. The flat-nose missile, on the other hand, penetrates with a lower velocity, but because of the serious damage due to the scabbing process, continues its progression to reach a greater depth.

It has been shown that for targets in which the ratio of the target thickness versus the missile diameter is approximately one, Chen and Li's prediction formulae [5] do not apply. The question then arises as to what happens when this ratio is greater than one, which means a thick target. To this end, a 0.8 m target thickness was generated with the DEM model, still using both, the same local parameters and configuration set for the reinforcement. Then the same sequence of impacts was performed. The results are shown in Fig. 10. It is now seen that for a thicker target, the conical

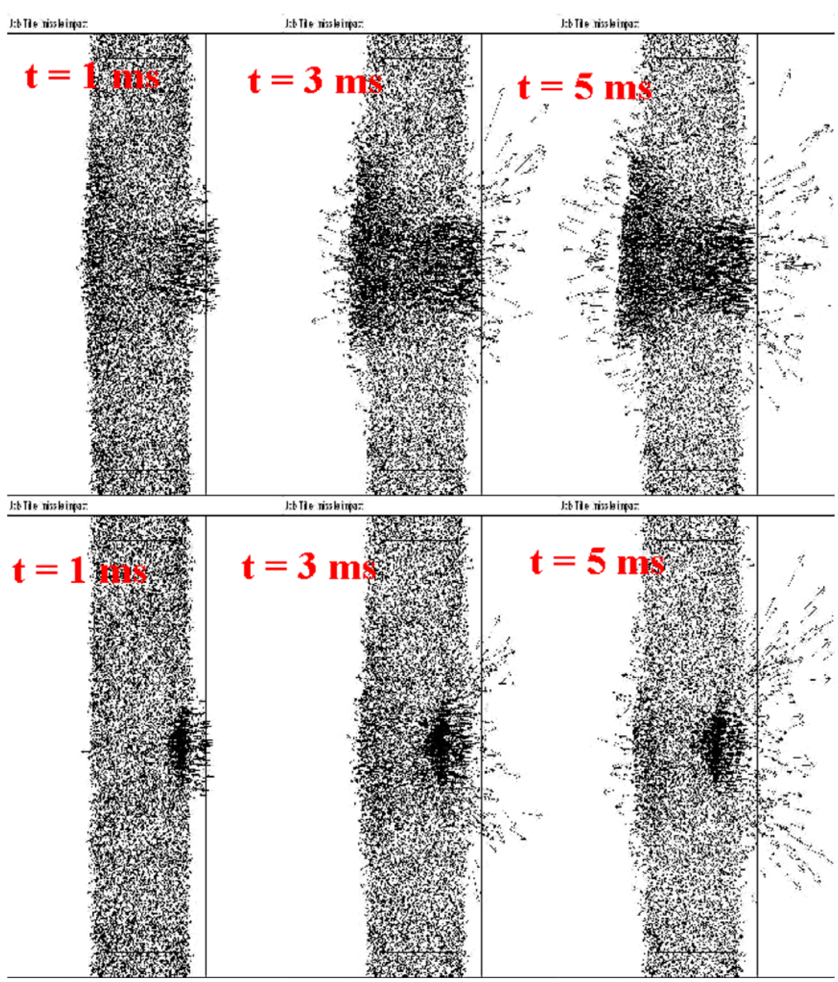

Fig. 9. Displacement vector snapshots in which the flat-nose is on the top view and a 10 cm conic-nose on the bottom view.

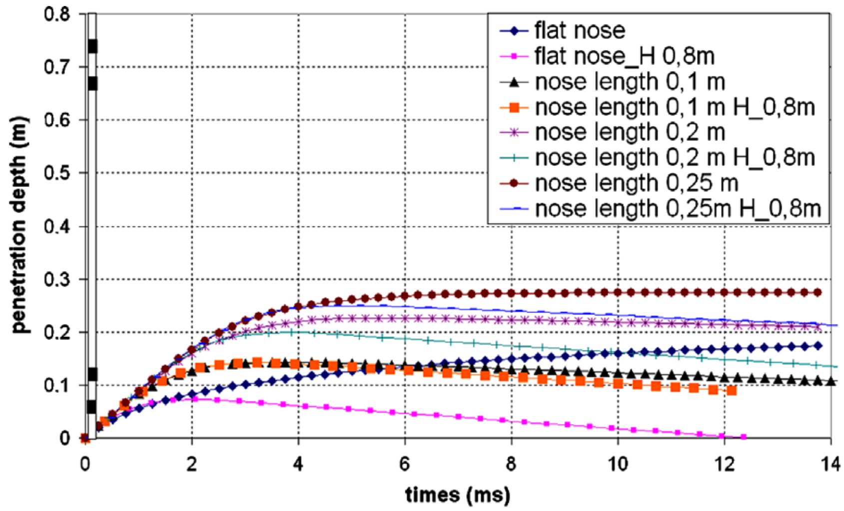

Fig. 10. Missile's trajectory history with target thickness of 0.4 m and 0.8 m (numerical results).

nose missiles penetrate more than the flat nose missile, which corresponds to Chen and Li's prediction formulae [5]. In these cases, scabbing is absent.

4. Conclusion

The main specificities of the 3D discrete element approach are the following: the modeling scale is higher than the heterogeneity scale, so the model may be used to simulate real structures, which means that the DEM is mainly used here for its ability to account for discontinuities; the interaction laws introduced are then very simple and are close to macroscopic laws; finally, an identification process based on quasi-static tests is used, so the quasi-static behavior of concrete is reproduced. This identification process is the key point, to allow a complete predictive computation.

In this work, the CEA-EDF impact tests were studied and simulated with this model, for different impact velocities, on a reinforced concrete slab at a real scale. Results were compared with experimental results: quantitatively results are very coherent with respect to experimental results. Moreover, by studying how the shape of the missile's nose affects the penetration depth, it has been shown that for targets in which the ratio of the target thickness versus the missile diameter is approximately one, Chen and Li's prediction formulae [5] do not apply, but the numerical and experimental data sets are within bounds of one another. When the thickness of the target is increased, the numerical results agree with Chen and Li's formulations.

References

[1] Adeli H, Amin AM. Local effects of impactors on concrete structures. Nucl Eng Des 1985;88:301–17.
[2] Bathe KJ, Walczak J, Welch A, Mistry N. Nonlinear analysis of concrete structures. Comput Struct 1989;32(3/4):563–90.
[3] Berriaud C, Sokolovsky A, Gueraud R, Dulac J, Labrot R. Local behavior of reinforced concrete walls under missile impact. Nucl Eng Des 1978;45(2):457–69.
[4] Camborde F, Mariotti C, Donzé FV. Numerical study of rock and concrete behavior by discrete element modeling. Comput Geotech 2000;27(4):225–47.
[5] Chen XW, Li QM. Deep penetration of a non-deformable projectile with different geometrical characteristics. Int J Impact Eng 2002;27:619–37.
[6] Cundall PA, Strack ODL. A discrete numerical model for granular assemblies. Géotechnique 1979;29(1):47–65.
[7] Degen PP. Perforation of reinforced concrete slabs by rigid missiles. J Struct Div 1980;106(7):1623–42.
[8] Donzé FV, Magnier SA, Daudeville L, Mariotti C, Davenne L. Study of the behavior of concrete at high strain rate compressions by a discrete element method. J Eng Mech 1999;125(10):1154–63.
[9] Hentz S, Daudeville L, Donzé FV. Identification and validation of a discrete element model for concrete. J Eng Mech 2004;130(6):709–19.
[10] Hughes G. Hard missile impact on reinforced concrete. Nucl Eng Des 1984;77(1):23–35.
[11] Itasca. PFC^{3D} (particle flow code in 3 dimensions), Version 3.0. Itasca Consulting Group Inc., Minneapolis, Minnesota; 2003.
[12] Iwashita K, Oda M. Micro-deformation mechanism of shear banding process based on modified distinct element method. Powder Technol 2000;109:192–205.
[13] Kennedy RP. Effect of an aircraft crash into a concrete reactor containment building. Holmes and Narver Inc., Anaheim, Californial; July1966.
[14] Li QM, Tong DJ. Perforation thickness and ballistic limit of concrete target subjected to rigid projectile impact. J Eng Mech 2003;129(9):1083–91.
[15] Li QM, Reid SR, Wen HM, Telford AR. Local impact effects of hard missiles on concrete targets. Int J Impact Eng 2006;32(1–4):224–84.
[16] Magnier SA, Donzé FV. Numerical simulations of impacts using a discrete element method. Mech Cohesive-Frictional Mater 1998;3(3):257–76.
[17] Masuya H, Kajikawa Y, Nakata Y. Application of the distinct element method to the analysis of the concrete members under impact. Nucl Eng Des 1994;150(2–3):367–77.
[18] Meguro K, Hakuno M. Fracture analyses of concrete structures by the modified distinct element method. Struct Eng/Earthquake Eng 1989;6(2):283–94.
[19] Potapov AA, Hopkins MA, Campbell CS. A two-dimensional dynamic simulation of solid fracture part I: description of the model. Int J Mod Phys 1995;6(3):371–98.
[20] Potyondy DO, Cundall PA, Lee CA. Modelling rock using bonded assemblies of circular particles. In: Proceedings of the second North American rock mechanics symposium. Rock mechanics tools and techniques. Montréal, June 1996. p. 1937–44.
[21] Riera JD, Iturrioz I. Discrete elements model for evaluating impact and impulsive response of reinforced concrete plates and shells subjected to impulsive loading. Nucl Eng Des 1998;179(2):135–44.
[22] Sliter GE. Assessment of empirical concrete impact formulas. J Struct Eng 1980;106:1023–45.